LUND UNIVERSITY

Nuclear potential-energy surfaces and the half-lives of heavy and super-heavy elements

Nilsson, Sven Gösta

Published in:
Computer Physics Communications

1972

Link to publication

Citation for published version (APA):
Nilsson, S. G. (1972). Nuclear potential-energy surfaces and the half-lives of heavy and super-heavy elements. *Computer Physics Communications*, (3), 92-116.

Total number of authors:
1

General rights
Unless other specific re-use rights are stated the following general rights apply:
Copyright and moral rights for the publications made accessible in the public portal are retained by the authors and/or other copyright owners and it is a condition of accessing publications that users recognise and abide by the legal requirements associated with these rights.
• Users may download and print one copy of any publication from the public portal for the purpose of private study or research.
• You may not further distribute the material or use it for any profit-making activity or commercial gain
• You may freely distribute the URL identifying the publication in the public portal

Read more about Creative commons licenses: https://creativecommons.org/licenses/

Take down policy
If you believe that this document breaches copyright please contact us providing details, and we will remove access to the work immediately and investigate your claim.

LUND UNIVERSITY

PO Box 117
221 00 Lund
+46 46-222 00 00

Download date: 17. Dec. 2025

F:502 51

COMPUTER PHYSICS COMMUNICATIONS 3, SUPPL. (1972) 92–116. NORTH-HOLLAND PUBLISHING COMPANY

NUCLEAR POTENTIAL-ENERGY SURFACES AND THE HALF-LIVES OF HEAVY AND SUPER-HEAVY ELEMENTS

Sven Gösta NILSSON
Lund Institute of Technology, Lund, Sweden

Received 17 April 1972

1. Introduction

The frontiers of nuclear physics have to-day to a fair extent to do with an extension of our knowledge of the nuclear potential-energy surface. With the term "potential energy" we denote conventionally the minimum nuclear energy associated with each shape. We thus exclude the energy associated with the collective motion, which latter we chose to consider specifically, and also the energy dissipated, after the penetration of the barrier, in form of nuclear "heat" or "viscous energy".

The fact that the nucleus may be associated with a shape – other than spherical – was first made apparent by the early investigations by Rainwater [1], by Brix and Kopferman [2] and by Bohr [3], and the concept of shape was first forcefully exploited by the Copenhagen school. The first deviations from sphericity considered were those associated with quadrupole shapes. At a very early stage also other degrees of freedom were considered by Bohr and Mottelson and their co-workers for the ground state shapes, as the octupole (ϵ_3) and then the hexadecapole (ϵ_4) degrees of freedom. It was found around 1955 that good equilibrium quadrupole (or ϵ-) distortions could be calculated simply by minimizing sums of single-particle energies. The same recipe was later found to work also for ϵ_4 equilibrium shapes under certain conditions. The latter sum $\epsilon = \Sigma_\nu e_\nu(\epsilon, \epsilon_4 ...)$ modified by pairing and Coulomb energies was found to describe the potential-energy surface well enough to indicate the possible existence of secondary fission isomer minima discovered a few years earlier by Flerov and Polikanov [4]. However, for a quantitative description it became apparent that an extra normalization was needed at the distortions involved in describing the second barrier peak. This was provided by the Strutinsky [5] shell correction method, which was found to be the indispensable tool long looked for to remedy the oversensitivity of the calculations to the volume conservation condition. Presently most calculations pertaining to the nuclear potential-energy surface rely on this method, the theoretical basis of which is now being better understood. For the calculations in accordance with this method one also relies on the average applicability at large distortions of the liquid-drop model. I shall come back to these points later.

The occurrence of minima in the potential-energy surface we thus associate with the deformed or spherical ground states and with fission isomeric states. The ground-state distortions usually vary from 0.4 to 0.2 in ϵ; the empirically identified fission shape isomers lie conspicuously near $\epsilon = 0.6$. One may look at fig. 1 to get an idea of the distortions involved.

2. The potential

To become a little more specific, we start from the following type of potential:

$$V = \tfrac{1}{2}\hbar\omega\rho^2(1 - \tfrac{2}{3}\epsilon P_2 + 2\epsilon_4 P_4 + 2\epsilon_3 P_3 + 2\epsilon_5 P_5)$$
$$+ C\bar{l}_t\bar{s} + D(\bar{l}_t^2 - \langle\bar{l}_t^2\rangle).$$

We actually also have to include a P_1 term in the asymmetric case, i.e., when P_3 and P_5 distortions are

Fysik -& astronomibiblioteket
Lunds universitet

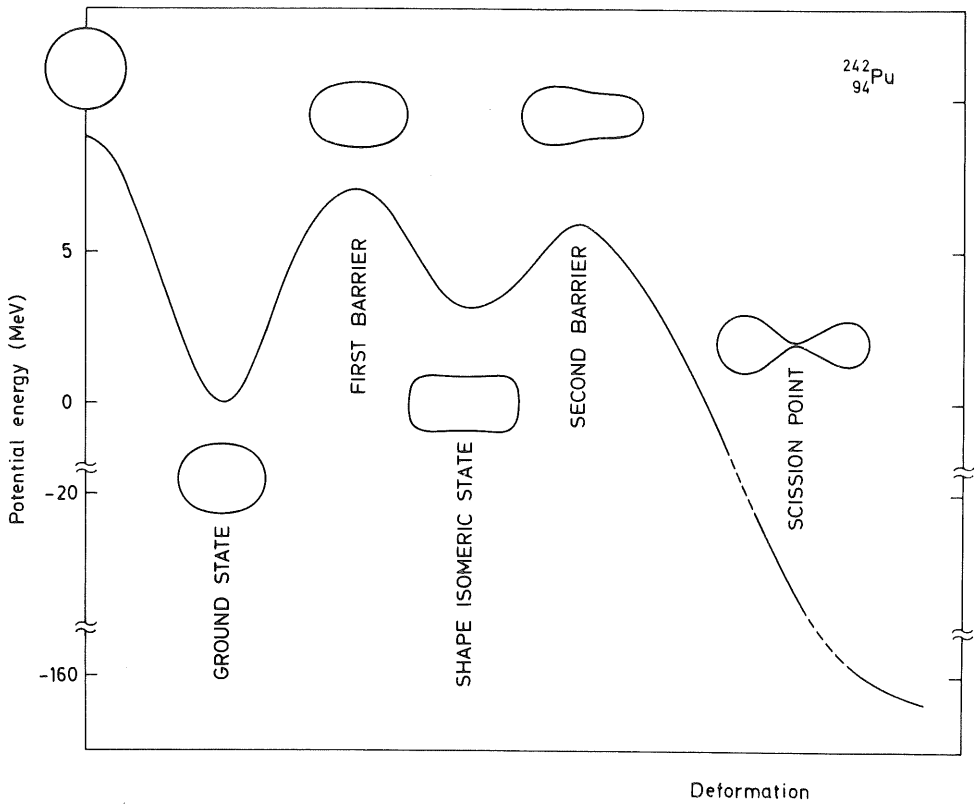

Fig. 1. The nuclear fission barrier as a function of deformation. Realistic deformation shapes are indicated in the figure above and below the barrier line.

considered, in order to compensate for a trivial center-of-mass displacement.

For the treatment of this modestly complicated potential, which goes back on an even simpler version that the author studied in the 1950's, the availability of computers has been found indispensable. The problem is there to find single-particle wavefunctions and energies for a large number of orbitals and corresponding to a large number of values of the shape parameters. For the further treatment of this calculational information the computer becomes even more useful. We are returning to this problem below.

At this point I should add that many other potentials and shape parametrizations are available. Maybe you find a Woods–Saxon well more physical. This or something rather similar has been parametrized all the way to scission according to very elegant parameter schemes by Nix et al. [6], by the Strutinsky group [7], and by Pashkevich [8]. The Pashkevich parametrization scheme, based on cassinian ovaloid shapes, is also very conveniently adapted to the oscillator potential.

Two-centre formulations using an oscillator with a bump added along the z axis, or two joined oscillators, have been proposed by Andersen et al. [9], Slavov et al. [10], Holzer et al. [11], Johansson [12], the latter a member of our group in Lund. All have their advantages over the potential I just wrote down, in particular when you approach the scission point. For more modest distortions, sufficient to describe heavy actinide and super-heavy element fission barriers out to the exit point, we believe the generalized oscillator mentioned here is still satisfactory. All of these modern potential variants are presently being treated with the help of computers.

Turning to the generalized oscillator again, the most recent interest is centered around the reflection asymmetric $P_3 + P_5$ terms and the addition of an axial

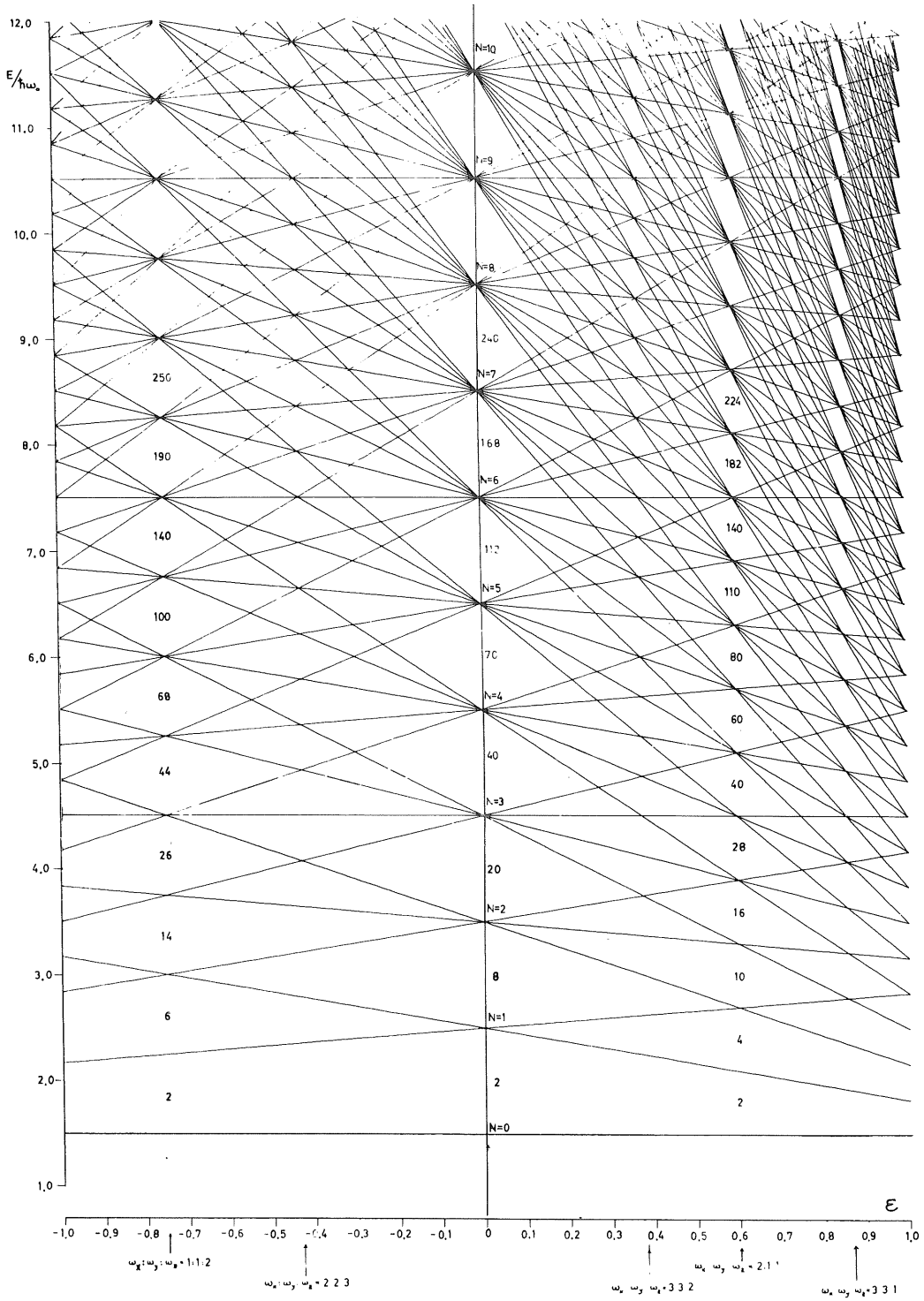

Fig. 2. Single-particle energies in an ellipsoidal harmonic oscillator potential as a function of the eccentricity parameter ϵ. Note, e.g., for $\epsilon = 0.6$, the ratio of axes being 1 : 1 : 2 (or the ratio of ω-values 2 : 2 : 1), there occur magic numbers as indicated in the diagram. Note similar shell effects associated with $\epsilon = -0.75$ and $\epsilon = 0.875$.

asymmetry term proportional to $(Y_{22} + Y_{2-2})$. The axial asymmetry problem is presently being treated by Ragnarsson and Larsson [13] in Lund and by Goetz et al. [14] in Basel. These were preceded by the exploring work by Pashkevich [15].

Let us first study the pure harmonic oscillator model the special case of the potential above with $\epsilon_3 = \epsilon_5 = \epsilon_4 = 0$. In terms of this

$$V_{\mathrm{osc}} \sim \omega_\perp^2(x^2 + y^2) + \omega_z^2 z^2.$$

The ratio of axes of the corresponding ellipsoid goes as

$$a/b = \omega_\perp/\omega_z = (1 + \tfrac{1}{3}\epsilon)/(1 - \tfrac{2}{3}\epsilon).$$

The ratio of axis lengths of 2 : 1 : 1 occurs for $\epsilon = 0.6$ on the prolate side and 1 : 2 : 2 for $\epsilon = -0.75$ on the oblate side.

If we turn to fig. 2, where single-particle energies are plotted in terms of ϵ, we notice strong shell effects first for the spherical case $\epsilon = 0$, then on the oblate side for $\epsilon = -0.75$ and on the prolate for $\epsilon = 0.6$. Weaker shell effects are associated with ratios of for instance 4 : 3 : 3, 5 : 3 : 3, 3 : 2 : 2. The energy associated with the harmonic oscillator can be written

$$E = (n_z + \tfrac{1}{2})\hbar\omega_z + (n_\perp + 1)\hbar\omega_\perp,$$

which for $\epsilon = 0.6$, when $\omega_z = \frac{1}{2}\omega_\perp = 0.6\,\omega_0$, goes over into

$$E - \tfrac{3}{2}\hbar\omega_0 = 0.6\hbar\omega_0(n_z + 2n_\perp) = 0.6\hbar\omega_0 n_2,$$

where thus

$$n_2 = n_z + 2n_\perp.$$

The energy spacing is thus given by n_2 and the degeneracy for even n_2 by $\frac{1}{4}(n_2 + 2)^2$, which should be compared to a degeneracy associated with N of $(N+1)(N+2)$. This is thus basically the same type of degeneracy as in the spherical case, and proportional to $A^{1/3}$. The degeneracy connected with the spherical Coulomb potential is also of this magnitude or $A^{1/3}$. Therefore this $\epsilon = 0.6$ degeneracy, as stressed by Bohr and Mottelson *, is a very important type of degeneracy. On the other hand the type of minimum that is associated with the rare-earth and actinide ground state reflects in part the spherical degeneracy in the case of half-filled shells, which thus gives a trend away from sphericity, and in part the influence of the shell effects associated with $\omega_\perp/\omega_z = 3:2$ or 4 : 3. The corresponding magic numbers are listed in fig. 3a.

The problem is how much of this shell structure that remains when spin–orbit and other corrections are added or when the oscillator is replaced with a Woods–Saxon potential. For the region of the periodic table where fission isomer states are found to occur, the corresponding shell is found to remain although displaced, the modifications being minor; thus $N = 140$ goes over into 148 or 146, etc. The existence of the latter magic number, relevant for fission isomeric shape distortion, was stressed at an early stage by Strutinsky.

One may study the shell correction energy $\Sigma e_\nu - \langle \Sigma e_\nu \rangle$ (see next section) as exhibited in fig. 3a for the pure h.o. potential for neutron values between $N = 100$ and $N = 200$. (The corresponding Z-values are chosen to lie along the stability line.) The magic numbers $N = 110, 140, 190$ connected with $\epsilon = 0.6$ are clearly brought out in the middle of large valleys in the (ϵ, N) plane. A large number of other gap effects are apparent.

In figs. 3b and 3c we exhibit the corresponding potential-energy surface for the case that the correction terms proportional to $l_t \cdot s$ and l_t^2 are added to the modified oscillator potential giving the three N-valleys from the previous figure. In addition pairing is included. Only the $N \approx 140$ valley is now clearly remaining on the prolate side above $N = 100$ though more shallow and also displaced to a somewhat larger N-value, or $N = 148$. Below $N = 160$ there exist experimental evidence relating to the h.o. gaps associated with $Z, N = 40$ and $N = 60$. The $N = 60$ gap is being displaced to $N = 64$ when $l \cdot s$ and l^2 terms are added.

Note that in fig. 3b we have assumed that the pairing matrix element is proportional to the area of the nuclear surface. This has as a consequence a general lowering of the potential-energy surface at large distortions, as is apparent in fig. 3b. In fig. 3c, on the other hand, G is assumed a constant independent of distortion.

* For much of this discussion the author is grateful for generous access to the manuscript of Bohr and Mottelson [16].

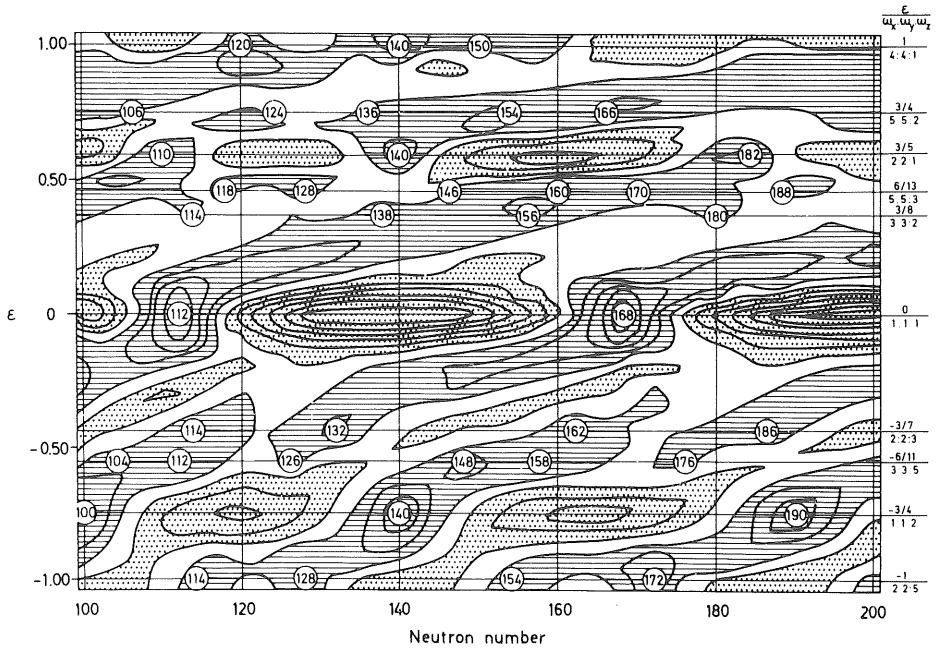

Fig. 3. (a) Neutron shell energy $\Sigma e_\nu - \langle \Sigma e_\nu \rangle$ exhibiting valleys (dashed areas) and mountain ridges (dotted areas), the former reflecting the closed-shell nucleon numbers of the previous figure. Note in particular the magic number 140 on the $\epsilon = 0.6$ and $\epsilon = -0.75$ oblate side. Contour line separation is 4 MeV.

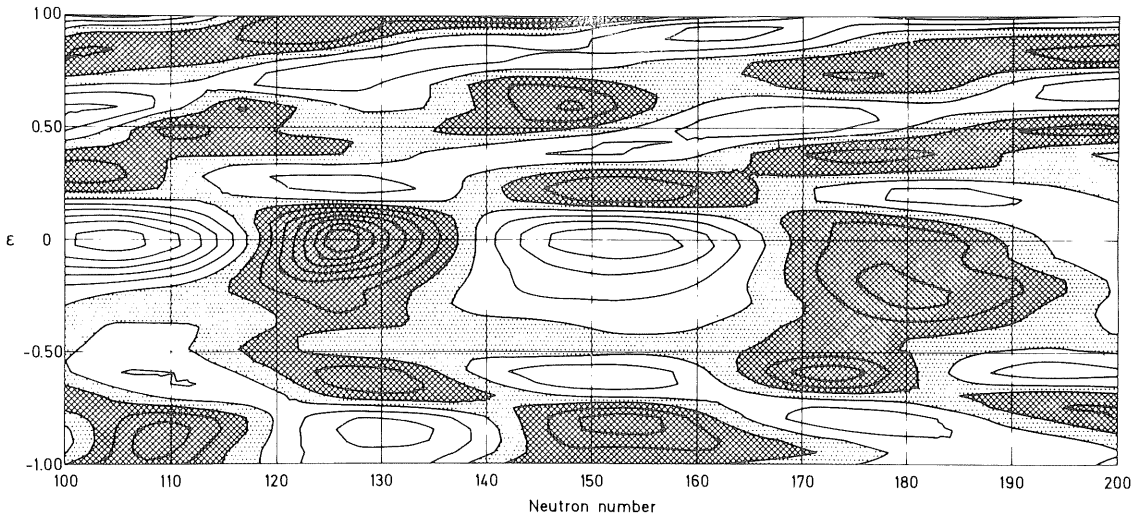

Fig. 3. (b) Neutron-pairing plus shell energy for the assumption of G = const. Contour line separation is here 1 MeV. The valleys and ridges of the previous figures are shifted by a few neutron numbers to slightly higher N-values.

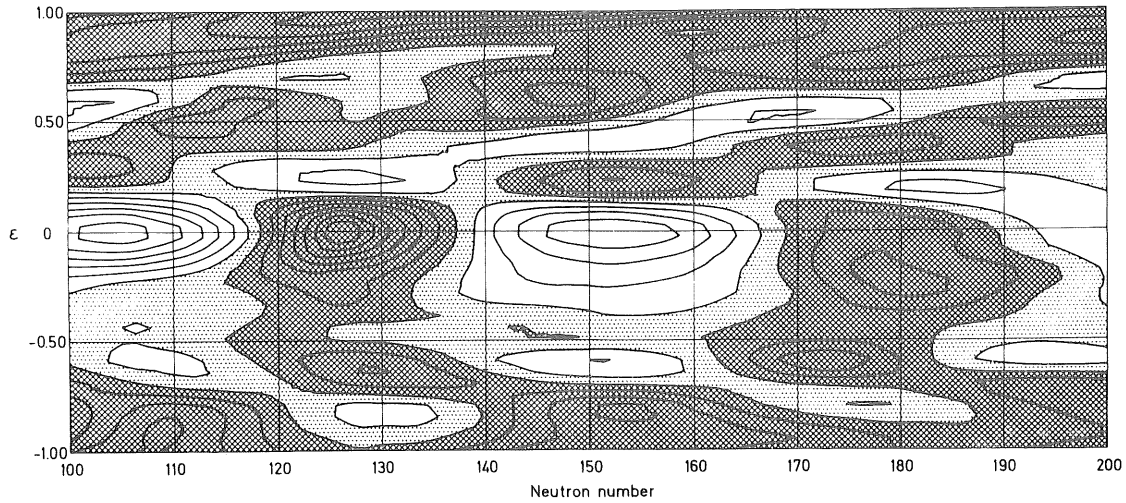

Fig. 3. (c) Same as fig. 3 (b) under the assumption of G proportional to surface area. (Figs. 3a–c are due to Mr. Ragnar Bengtsson, unpublished calculations.)

3. The Strutinsky or alternative procedures

Given the potential, we have to apply the method suggested by Strutinsky [5] to obtain from that an energy surface as is shown in figs. 4 and 5. The method of calculation according to this recipe is the following: the total energy is to be calculated as a smooth liquid drop energy supplemented by a term representing shell structure. The latter is the sum of the real single-particle energies minus a background of smeared energy levels

$$E_{\text{shell}} = \sum e_\nu - \langle \sum e_\nu \rangle .$$

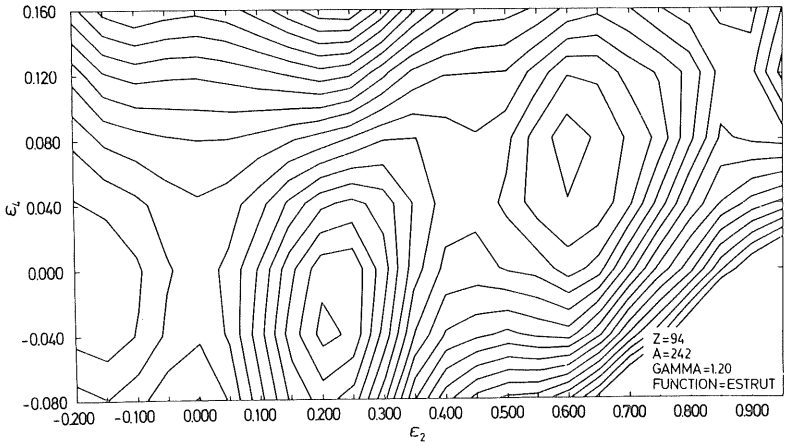

Fig. 4. (a) The nuclear potential-energy surface for $^{242}_{94}$Pu with shell, pairing and liquid-drop energies added, in terms of ϵ_2 (elongation) and ϵ_4 (waist-line coordinate). The lowest minimum at $\epsilon_2 \approx 0.21$, $\epsilon_4 \approx -0.04$ corresponds to the ground state (showing an ellipsoidal deformation). Note the secondary minimum at $\epsilon_2 \approx 0.6$. Note also that we use the notations ϵ and ϵ_2 for the quadrupole variable interchangeably throughout the text.

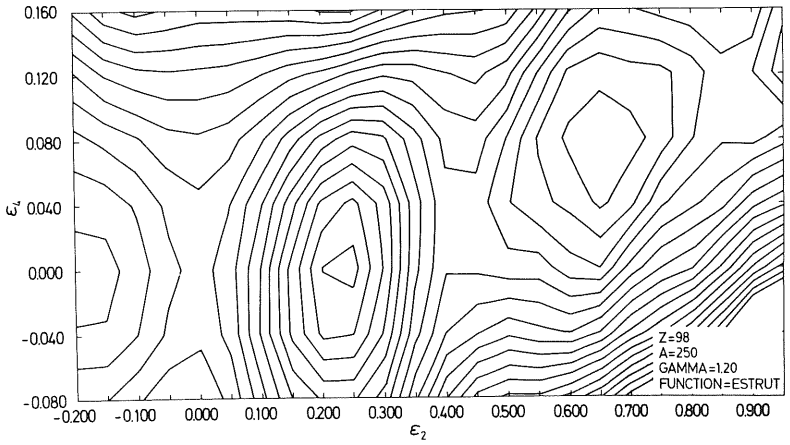

Fig. 4. (b) Same as fig. 4. (a) for $^{250}_{98}$Cf.

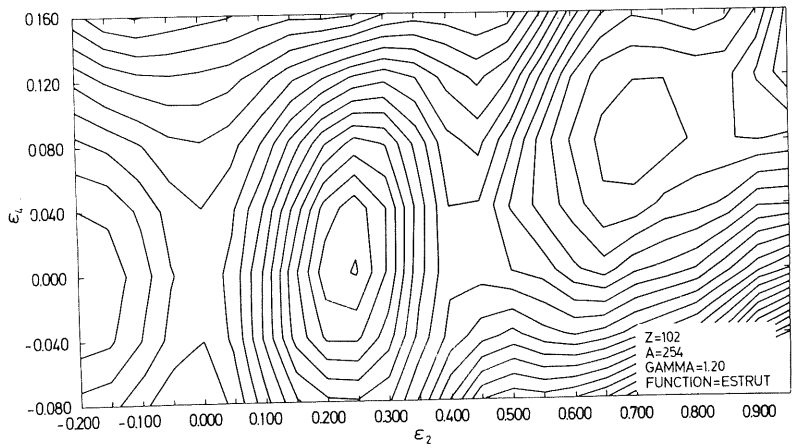

Fig. 4. (c) Same as fig. 4. (a) for $^{254}_{102}$No.

A central problem is how this background is to be estimated. Bohr and Mottelson in the new version of Vol. II of their monograph [16] recommend three avenues, alternative to the use of the Strutinsky smearing function.

(1) Let $A \to \infty$ and try to isolate terms proportional to A, $A^{2/3}$, $A^{1/3}$, etc. What remains after the subtraction of these gross structure terms is the shell correction term.

(2) Let T be large. For sufficiently large temperature T, the total energy or, even better, the free energy becomes a smooth function of T, which can be extrapolated back to $T = 0$. The difference between actual and extrapolated energies is the shell energy. Moretto [17] is presently exploring a similar method of calculating a shell correction term.

(3) Let ϵ be large. By a study of the summed single-particle energies as functions of ϵ one should be able to isolate the long-range behaviour of, e.g., the shell-correction and surface-energy terms.

A combination of (1) and (3) has also been suggested earlier by Swiatecki and Tsang [18].

Methods (1) and (2) are at the present being studied

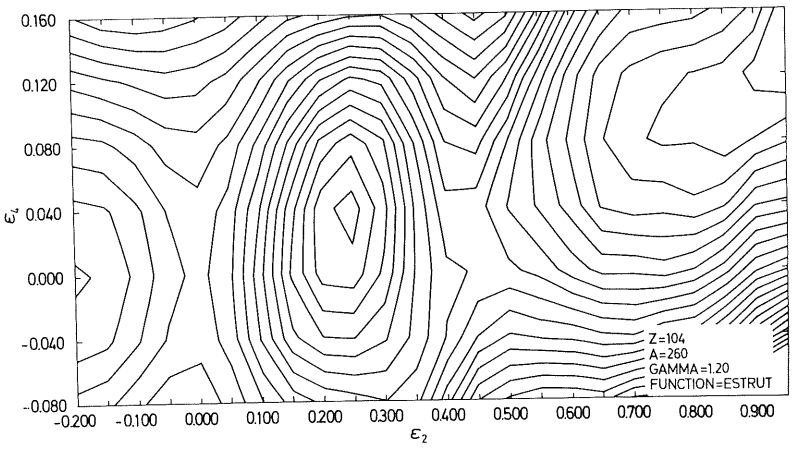

Fig. 4. (d) Same as fig. 4.(a) for $^{260}_{104}$Ku.

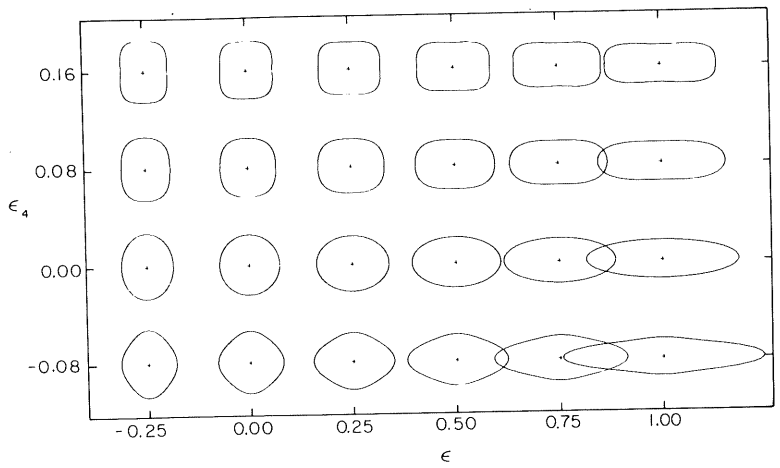

Fig. 5. Nuclear shapes as functions of ϵ and ϵ_4.

in Lund and Copenhagen. It appears that the success of (1) for the type of nuclear potential here considered is dependent on the prescribed behaviour of the κ and μ coefficients at (multiplying $l \cdot s$ and l^2) large A-values.

These are all from a physical viewpoint more attractive methods than that suggested by Strutinsky. The method developed by him remains for the moment the most explored and probably therefore the safest. The mathematics suggested by Strutinsky can only be implemented in practical cases through the use of computers. Given E_{shell} you obtain the total energy W as

$$W = E_{\text{shell}} + E_{\text{pair}} + E_{\text{surf}} + E_{\text{coul}},$$

i.e., by adding to E_{shell} the pairing term and the surface and Coulomb terms. In obtaining E_{shell} we have thus used the Strutinsky method in the calculations here presented although the alternative avenues are presently being explored.

4. Results of calculations using ϵ, ϵ_4 shapes

Some results of the calculations obtained by Tsang, myself and co-workers [19] in 1968 for the potential-energy surfaces for a series of actinide elements are given in figs. 4a–d. The coordinates then employed only involve ϵ and ϵ_4 coordinates. The first one thus represents nuclear elongation while ϵ_4 measures the "waistline" developed relative to the spheroid. The shapes then considered are shown in fig. 5.

In summary we should note first the double peaked character of the fission barrier for Pu and Cm while for larger Z- and N-values the second barrier is eroded.

For the super-heavy element nuclei a considerable fission barrier is restored because the ground-state shape becomes spherical. The barrier of $^{298}114$ has a height and a width comparable to that of ^{242}Pu.

5. The asymmetric degrees of freedom

I shall spend some time commenting on the problem of the influence of the asymmetric coordinates along the fission barrier. The problem given to us by experiments is, Why is some fission asymmetric and some symmetric? In other words, Why is the fragment mass distribution of $_{84}$Po fission symmetric, $_{92}$U fission strongly asymmetric and $_{100}$Fm fission weakly asymmetric (figs. 6, 7)? We shall for the moment posit that the answer has to do with the statical features, i.e., with the energy surface and in particular with the

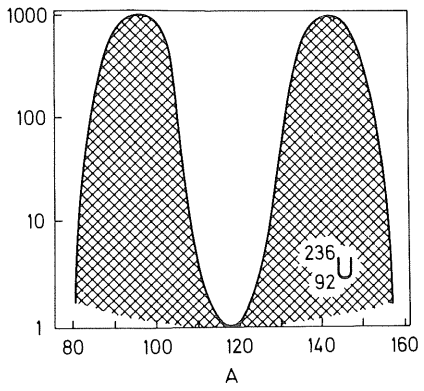

Fig. 6. Mass distribution of emitted fragments in the thermal fission of $^{236}_{92}$U.

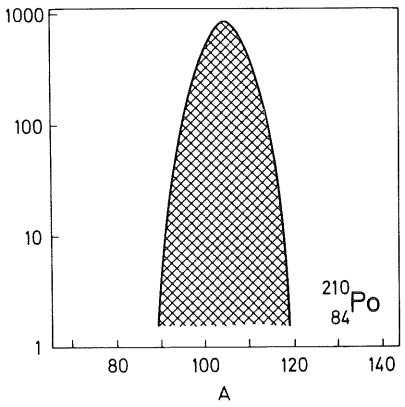

Fig. 7. Mass distribution of fragments in relatively low-energy fission of $^{210}_{84}$Po.

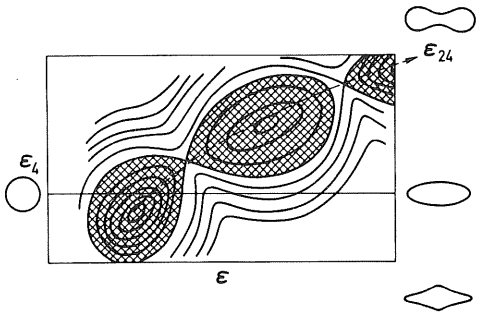

Fig. 8. Introduction of the coordinate ϵ_{24}, denoting corresponding elongation (ϵ) and waist-line (ϵ_4) shape coordinates along the "path to fission".

part of the surface that lies near the saddles. Look first in the (ϵ_2, ϵ_4) plane (fig. 8). Then introduce ϵ_{24} as a new axis and also ϵ_{35}, the latter referring to a linear combination of ϵ_3 and ϵ_5. The new plots as shown in figs. 9, 10, 11 and 12 are now in terms of ϵ_{24} and ϵ_{35} relevant to U and Po*. In these figures we give the resulting potential-energy surface when the ϵ (and ϵ_4) on the one hand, and ϵ_3 (and ϵ_5) on the other, are taken into account [20]. Fig. 11 is a photograph of a model constructed in soft-wood from the computer contour diagram. Direct computer

* The availability of computers for the exploration of this distortion space for a large number of nuclei is obviously a basic requirement for this type of approach.

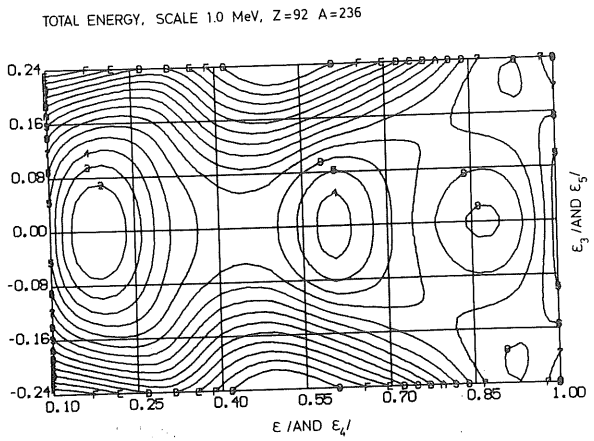

Fig. 9. Nuclear potential-energy surface for $^{236}_{92}$U in terms of ϵ_{24}, here denoted "ϵ (and ϵ_4)", and the asymmetric coordinate, here denoted "ϵ_3 (and ϵ_5)". The ground state is shown to the left. The "path to fission" is symmetric all the way to the second barrier, where there is a 2 MeV gain due to asymmetry.

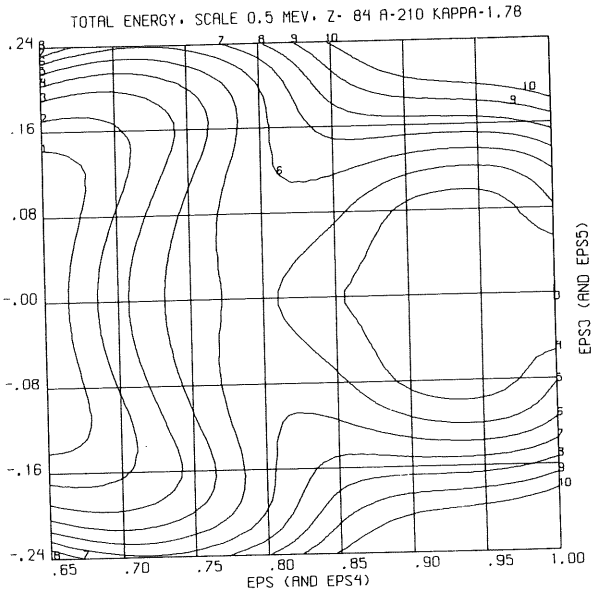

Fig. 10. Same as fig. 9 for $^{210}_{84}$Po.

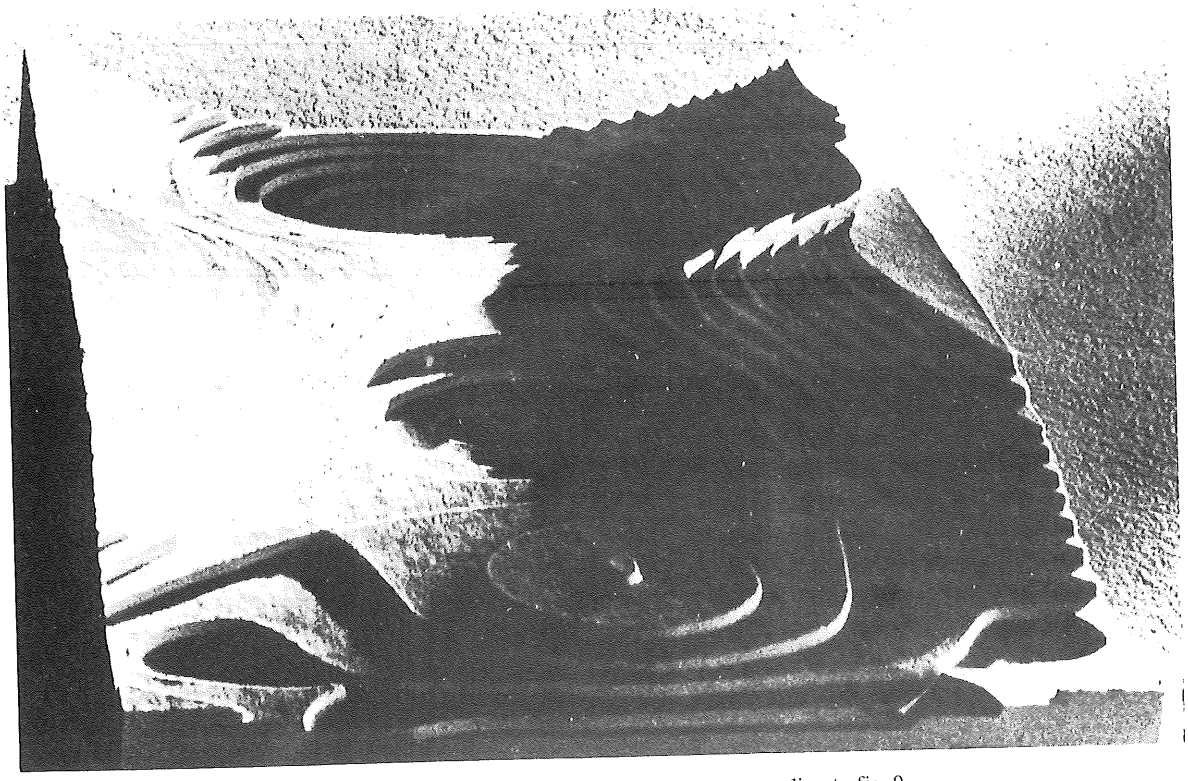

Fig. 11. A three-dimensional model surface corresponding to fig. 9.

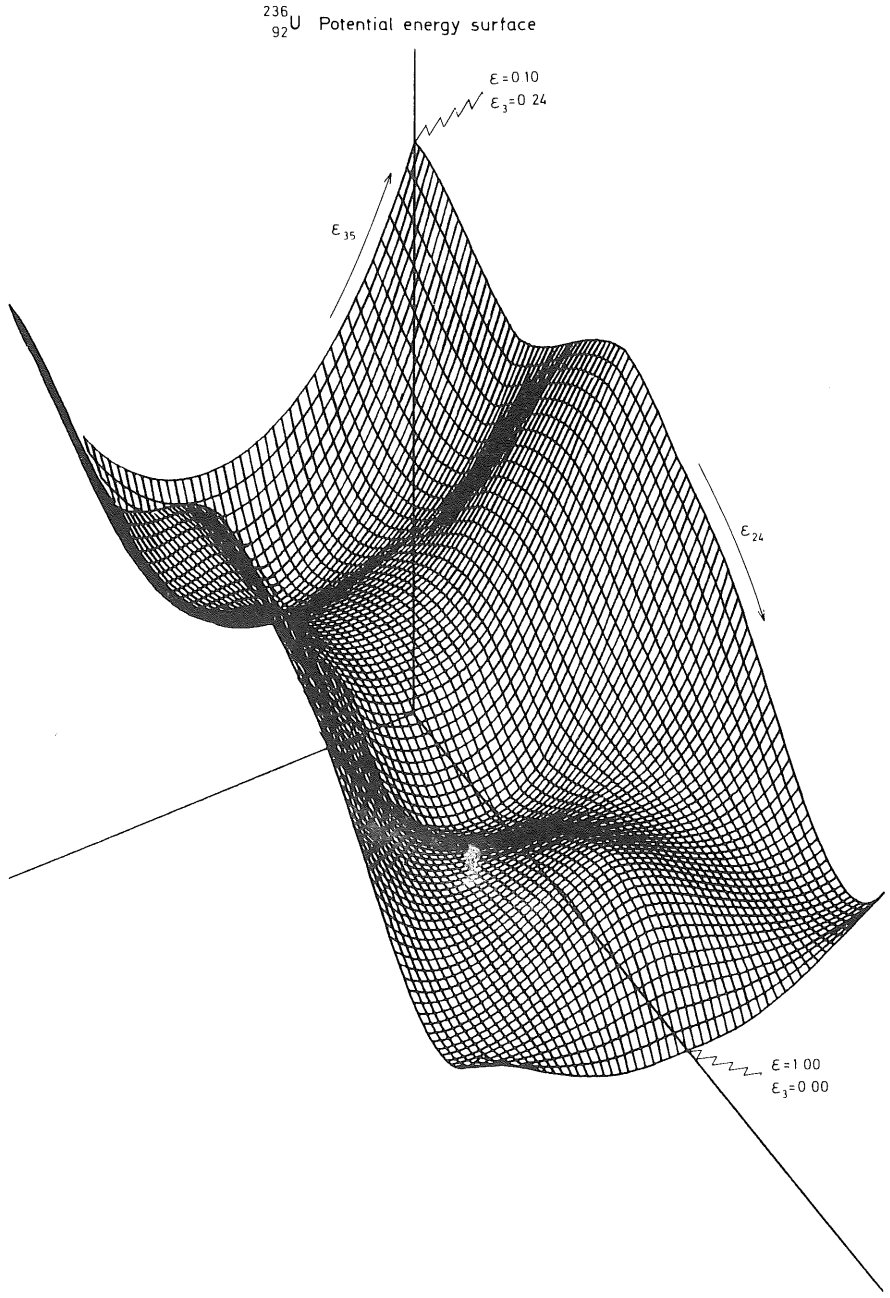

Fig. 12. Alternative representation of figs. 9 and 11.

projections of three-dimensional diagrams as fig. 12 are less illustrative than the photograph of the real three-dimensional model in this case.

Experimentally there is a transition region connected with some elements of Ra. Theoretically the energy surfaces of Rd and Ra, particularly those for the lighter isotopes of these elements, have indeed a transitional character showing three valleys and thus being intermediate between the symmetric-valley and two-asymmetric-valley cases. Let us for illustration turn to fig. 13. One may actually attempt to explain the well-known three-peak distribution of the mass fragments obtained experimentally for ^{227}Ac on the basis of this static surface as shown by Tsang and Wilhelmy [21]. One must note, however, some deficiency of the calculations, as the transition region is not associated with the correct but rather a somewhat smaller neutron number.

Along the stability line the relation of the second to the first peak is very favourably reproduced in these calculations. For most of these nuclei only the second barrier is affected by asymmetry. A maximal shell effect is encountered for the first peak for

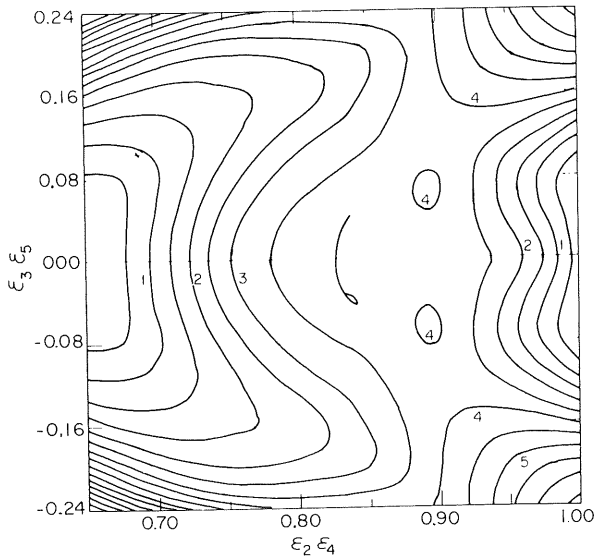

Fig. 13. The potential-energy surface around the second barrier for $^{228}_{88}$Ra in terms of ϵ (ϵ_4) and ϵ_3 (ϵ_5), under the assumptions of G = const., κ_S = 2.53. Note the three valleys. (Figure constructed by C.F. Tsang, who has also made small additions in the center of the figure as a work of art.)

$N \approx 156$ and for the second peak for $N \approx 146$. We have tried to understand the microscopic mechanism of the occurrence of instabilities in certain regions of mass and distortion, by trying to relate asymmetric instabilities to the appearance of certain nucleon orbitals [22] in the calculations. Here the computer was very helpful in saving us a lot of work. We simply plotted (fig. 14) the single-particle orbitals as a function of asymmetric deformation (ϵ_3). It is then easy to single out a few orbitals that respond particularly favourable to the distortion brought on from the outisde. These orbitals are marked [400 1/2], [402 3/2], [402 5/2], [404 7/2], etc., where the notation is the usual "asymptotic" one or $[Nn_z \Lambda\Omega]$, denoting total number of oscillator quanta (N), quanta along z axis (n_z) the z component of $l(\Lambda)$ and the z component of j (or Ω). The orbitals that seem to bend upwards from the interaction with those are [510 1/2], [512 3/2], [512 5/2], [514 7/2] etc. These pairs of orbitals are obviously the ones with strong matrix elements of $r^3 Y_{30}$ in between each other. A situation favourable to asymmetric distortion is the one where the former orbitals are filled and the latter empty. The most favourable situation just occurs for neutrons for $\epsilon \approx 0.8$ and $N \approx 142$ (fig. 15). The inclusion of the ϵ_4 degree of freedom additionally magnifies the effect by bringing the orbitals closer to each other. One of the downward bending orbitals [404 7/2] of fig. 14, plotted in configuration space, is illustrated in fig. 16, where the one orbital to which it couples most strongly, [514 7/2] is also exhibited.

The first barrier is usually stable, largely because of the stronger liquid-drop stabilities to asymmetric distortions at smaller elongations. What then about the orbitals near the secondary minimum, $\epsilon \approx 0.65$, of the actinides? For the latter case there is just the orbital [505 11/2] which itself is not enough to lead to asymmetry (except possibly in a few rare cases). We may foresee such a favourable situation for asymmetry at $\epsilon \approx 0.5$–0.6 for $N \approx 110$. Thus the secondary minimum of ^{190}Os, if it is axially stable, could well be asymmetrically unstable, which effect might serve to lower the minimum and make it more prominent. However, as no calculations are available presently, this should be regarded as a mere speculative suggestion.

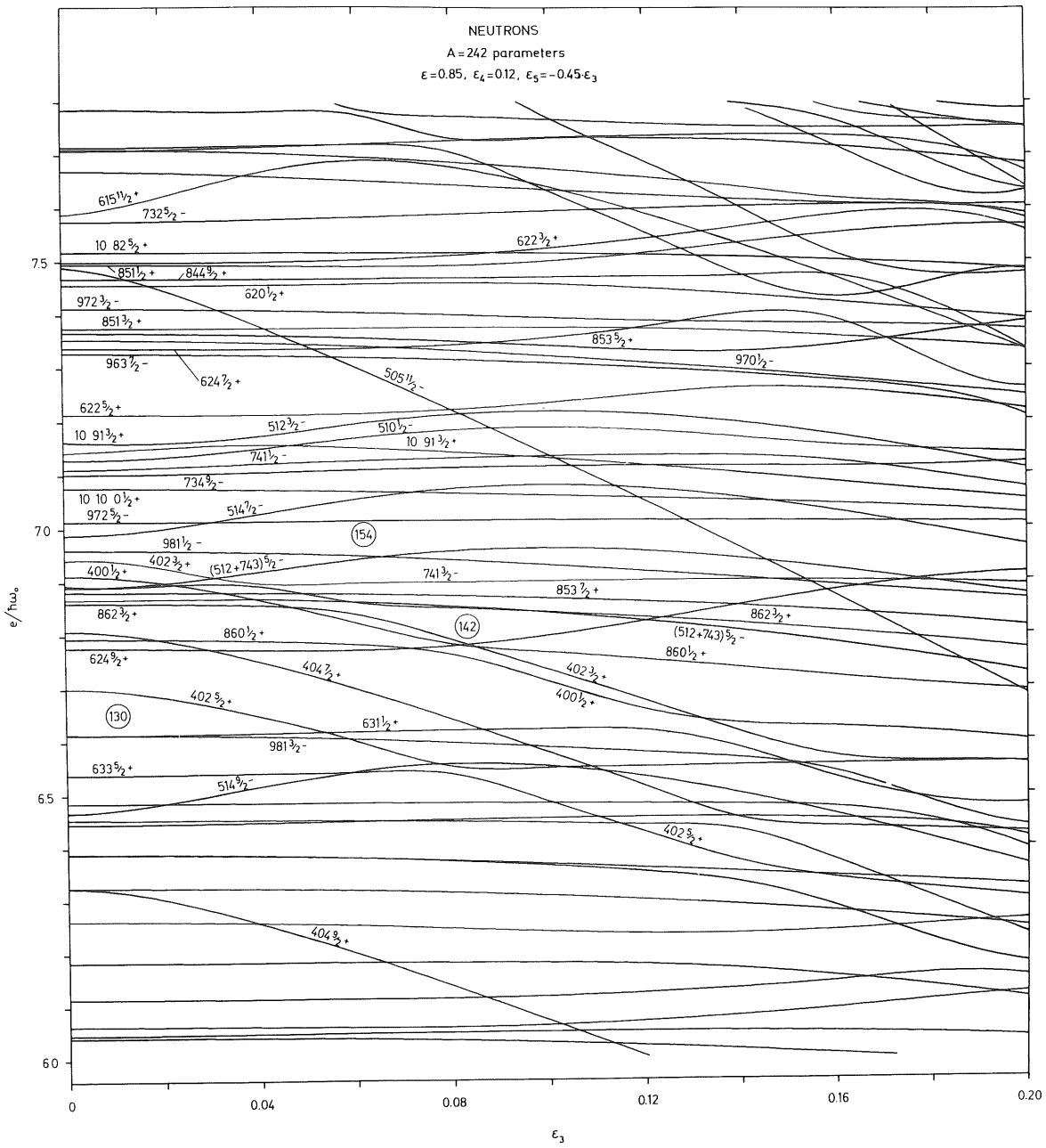

Fig. 14. Single-neutron orbitals for deformations appropriate at the second peak as functions of asymmetry ϵ_3. Note the down-curving orbitals [404 9/2], [402 5/2], [402 3/2], [400 1/2], [404 7/2], [505 11/2], etc., where notation is $[Nn_z\Lambda\Omega]$.

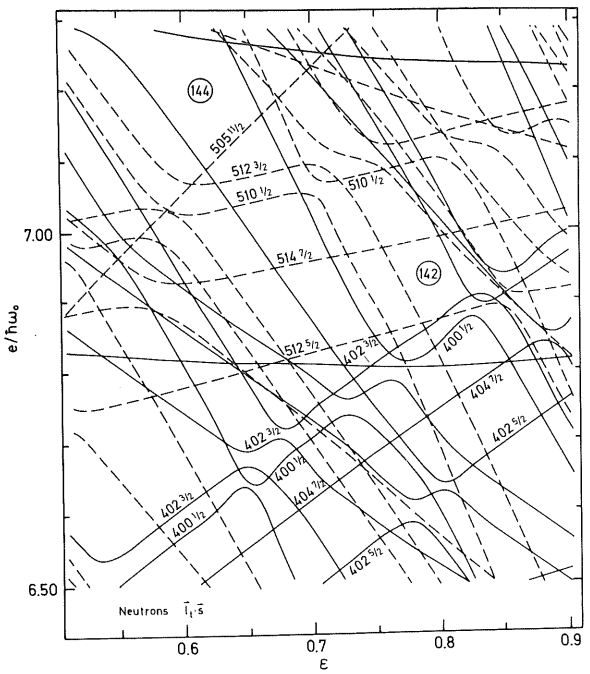

Fig. 15. The same single-neutron orbitals for deformations appropriate at the second peak as functions of $\epsilon(\epsilon_4)$. The second peak corresponds to $\epsilon = 0.8$.

6. Rotational asymmetry

In the above discussion of nuclear shapes only deformations that preserve rotational symmetry have been included. There are, however, strong indications from the Os, Pt region of nuclei that gamma asymmetric shapes are of importance. For the problem of the fission barrier these degrees of freedom were first taken into consideration by Pashkevich [15].

Recently we have added a term proportional to $\epsilon \sin\gamma(Y_{22} + Y_{2-2})$ to the potential above while modifying the ϵY_{20} term to $\epsilon \cos\gamma\, Y_{20}$. In this way for $\gamma = 0$ the axially symmetric case is restored while for $\gamma = 60$ in the pure ellipsoidal case an axially symmetric though oblately shaped potential is generated.

Some potential-energy surfaces in a plane (ϵ, γ), with other ϵ-parameters set = 0, for a sequence of isotopes of W are exhibited in fig. 17. Note the gradual transition from prolate to oblate shapes*.

* The addition of the ϵ_4 degree of freedom with unchanged s.p. parameters probably leads to a postponement of the prolate to oblate transitions to somewhat higher A values than $A \approx 190$.

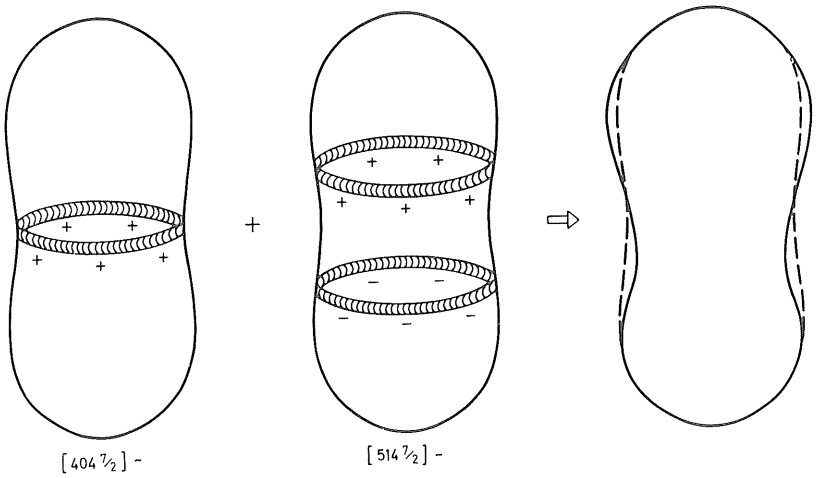

Fig. 16. Picture of an example of the mechanism of asymmetric distortions. Orbitals that couple are illustrated by [4 0 4 7/2] and [5 1 4 7/2].

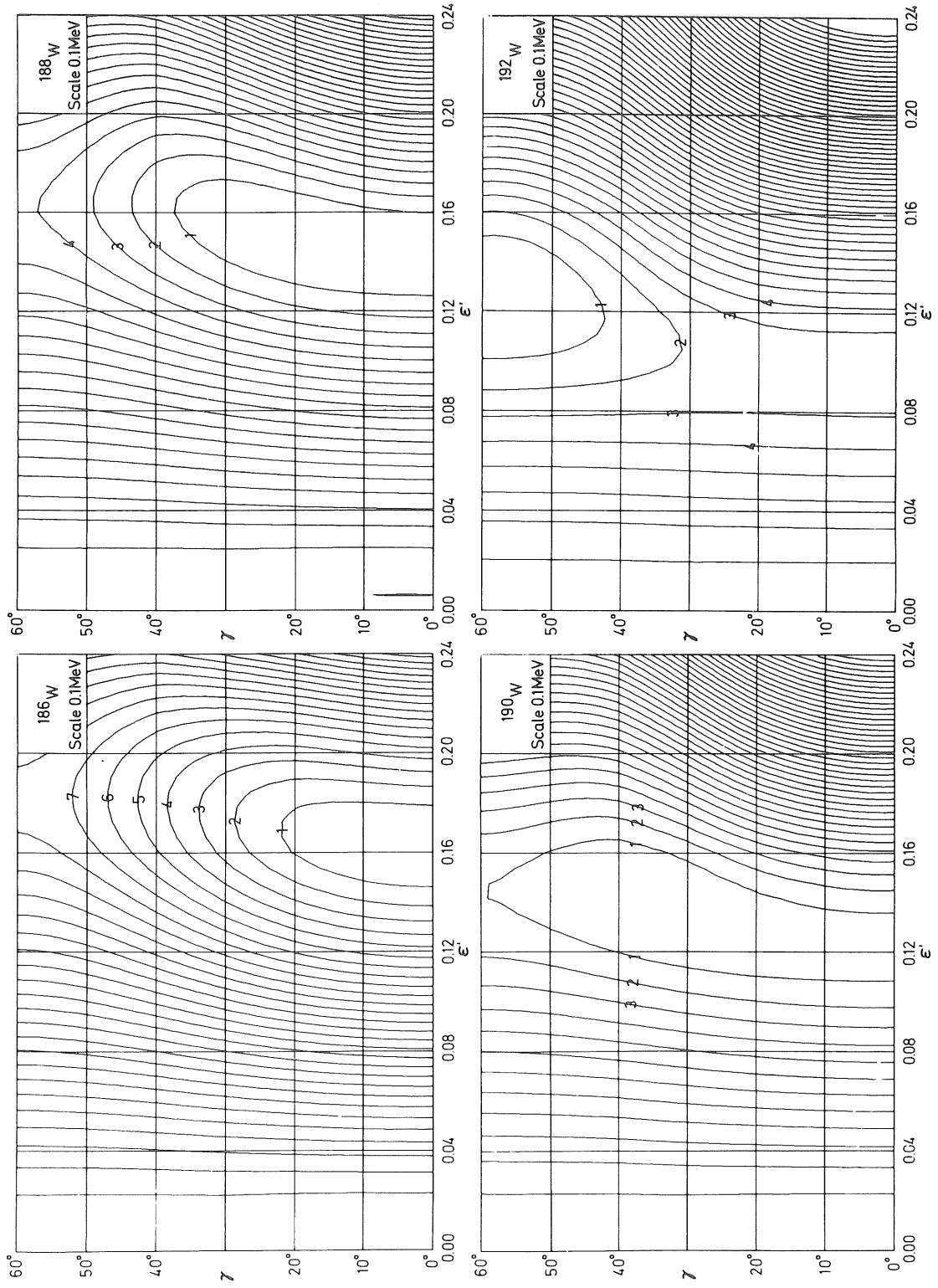

Fig. 17. Potential-energy surface for isotopes of $_{74}$W in terms of the deformation parameters ϵ and γ.

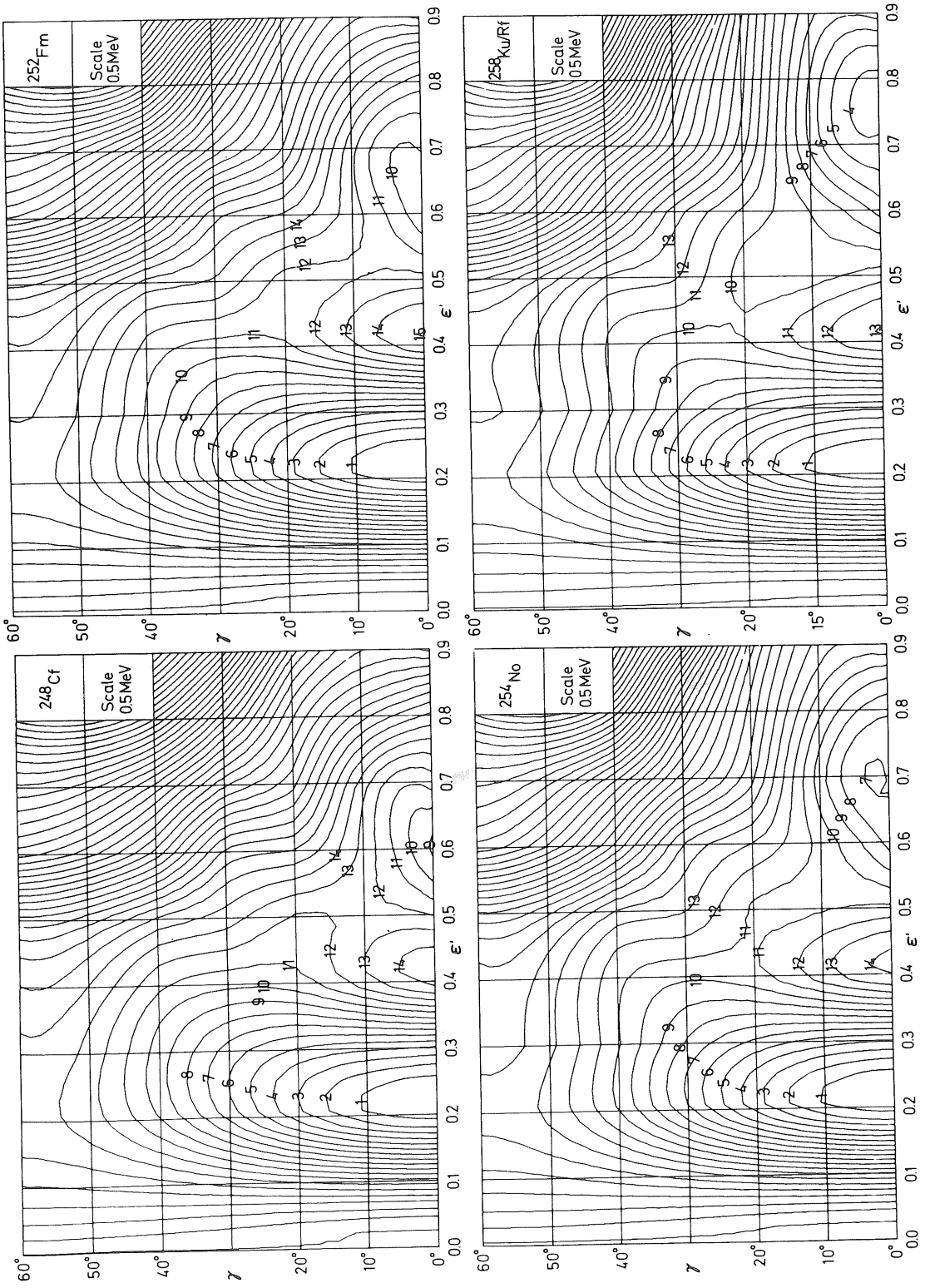

Fig. 18. Same as fig. 17 but for some representative actinide nuclei. Note the increased effect of γ on the height of the inner barrier.

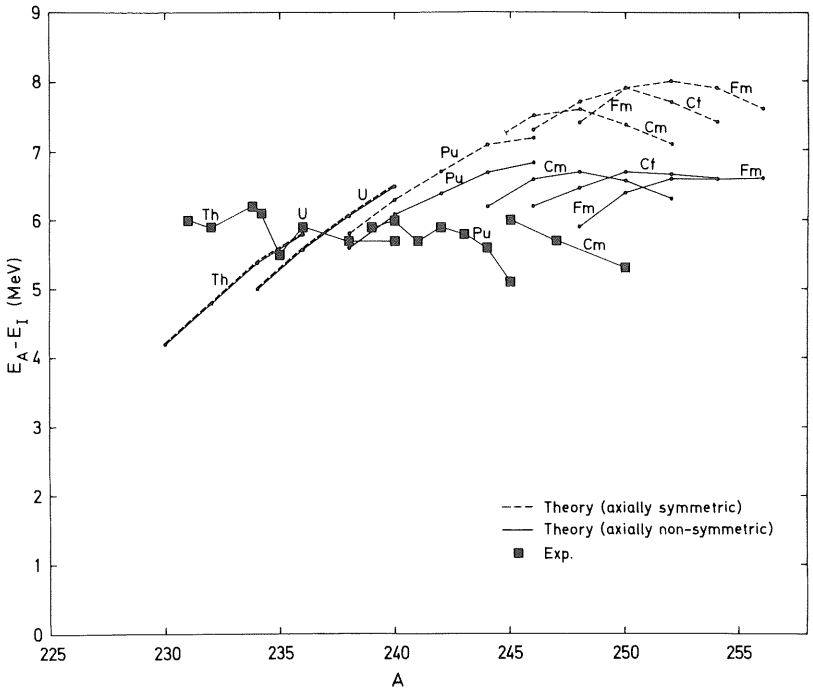

Fig. 19. (a) The height of the inner barrier experimentally and theoretically. Note the much improved agreement when γ is included.

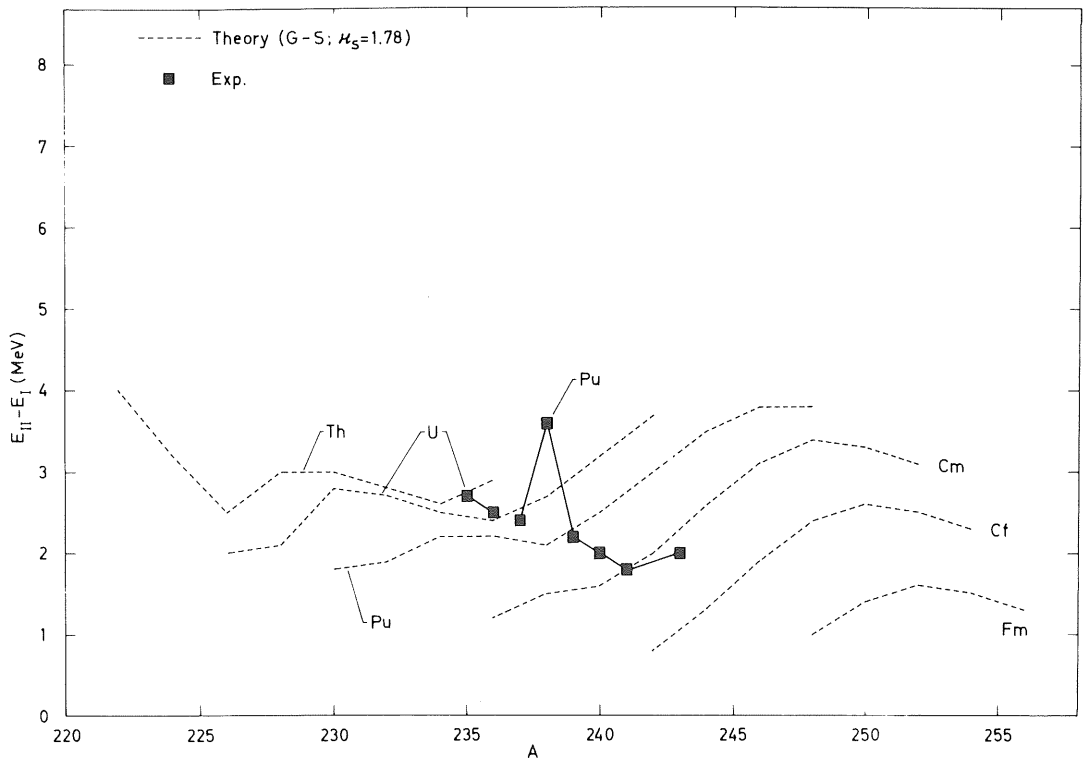

Fig. 19. (b) The energy of the second minimum theoretically and experimentally.

Fig. 18. Same as Fig. 17 but for some representative actinide nuclei. Note the increased effect of γ on the height of the inner barrier.

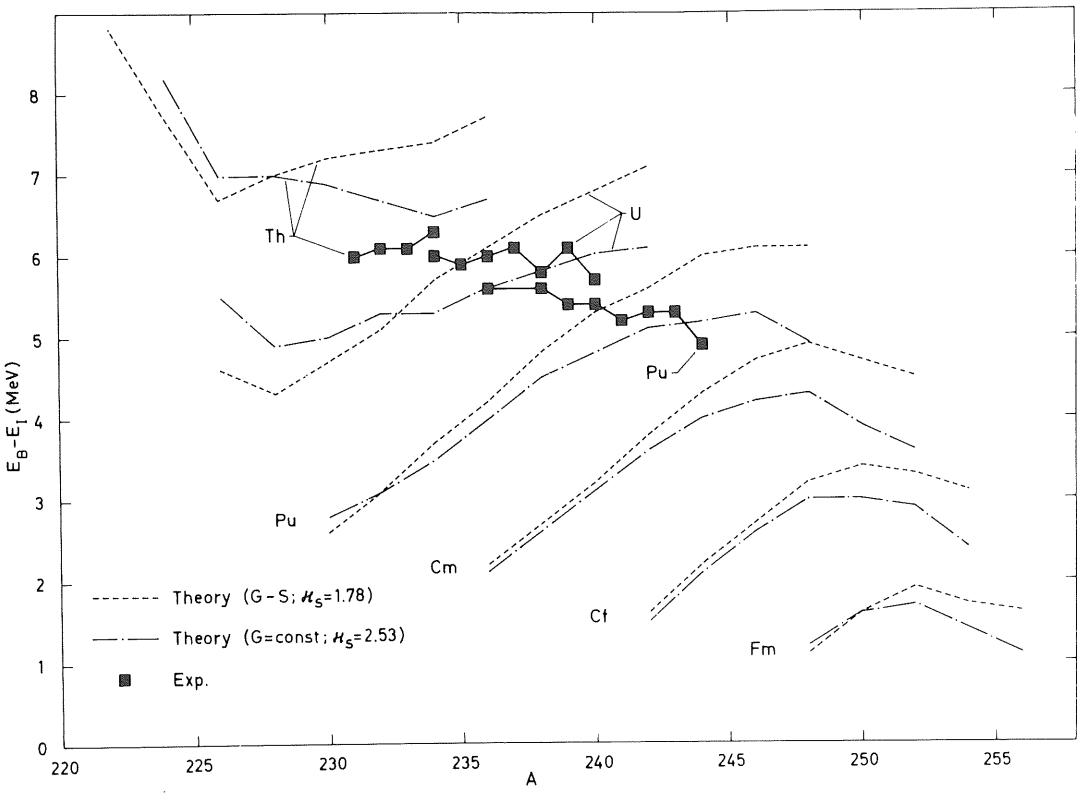

Fig. 19. (c) The height of the second barrier experimentally and theoretically.

The influence of the gamma degree of freedom [13] on the fission barriers of some actinide elements is shown in fig. 18. The reduction of the inner barrier due to gamma is strongest for the heavier actinides. The role of gamma in the super-heavy element region is similar to that for the actinides and causes a reduction of the inner barrier by up to 1.5 MeV.

7. Barrier characteristics

With the inclusion of the asymmetric degrees of freedom we have obtained a considerable lowering of the second saddle points. Similarly the inclusion of the gamma degree of freedom serves to lower the first barrier. Both effects serve to improve the agreement with experiments. It may be appropriate to summarize on the one hand the theoretical, on the other hand the experimental information as to the heights of the two barrier peaks and the energy of the secondary minimum relative to the ground state. This is done in fig. 19a (first barrier), 19b (secondary minimum), and 19c (second barrier).

The experimental data have been collected by Björnholm and Lynn [23]. The theoretical results represent those obtained by Larsson et al. in 1972 for the first barrier [13]. The theoretical results remain unchanged since the Nilsson et al. [19] 1968 calculations as to the second minimum, while the second barrier as obtained by Möller [24] is reduced by an amount up to 3 MeV relative to the 1968 calculations, due to the inclusion of $P_3 + P_5$ asymmetry.

The agreement with the data is actually somewhat better for the second barrier than for the first. While the theoretical values for elements along the stability line, as ^{236}U and ^{240}Pu, are very satisfactory, the trend with N for isotopes of any one of those elements is not as satisfactorily reproduced. This may

reflect in part on the use of improper values of the isospin dependent liquid-drop terms. The largest part of the effect is, however, probably due to some defects in the single-particle level diagram.

Recently, Pauli and Ledergerber [25] have varied the fissility parameter or the ratio of Coulomb to surface energy freely, thereby somewhat improving the fit to experiment of the barrier heights. In general, the erroneous isotopic trend with N of the theoretical results appears to remain, however.

8. A few words about SHE (super-heavy elements)

The early calculations by Tsang and myself [19] and the other people of the Lund and Warsaw groups predicted an island of SHE's as of fig. 20. The fission half-life determinations rest largely on our capability of calculating good potential-energy surfaces, i.e., proper barriers. These calculations have been carried through for more sophisticated types of potentials, by Strutinsky, Pauli et al. [7], and by Nix et al. [6]. While our fission barrier comes out 10 MeV high for $^{298}114$, the latter authors obtain barrier heights of almost 13 MeV. Consequently Strutinsky, Pauli et al. also end up with fission half-lives of up to 10^{30-40} years where we have 10^{14} years or so, the estimate being highly dependent on what is assumed about the mass parameters. Nix et al. on the other hand, who use semi-empirical inertial parameters extrapolated from the actinide region, find fission half-lives in gross agreement with those obtained by us although somewhat longer. For the case of longer fission half-lives, alpha decay becomes the more decisive decay mode. With inclusion of alpha and beta decay Nix supports our early finding that $^{294}110$ is the most stable of the SHE nuclei. His estimate of the total half-life as being of the order of 2×10^9 years differs by only a factor of 10 from our estimates. The difference in the estimates of barrier heights reflects on the single-particle potential parameters in addition to the different type of spin–orbit term used. The shell model parameters in turn are largely dependent on the selection of a nuclear mass region where they are effectively fitted. Thus our potential-parameter values derive largely from the requirements to reproduce observed empirical spin sequences in the rare-earth and actinide regions while, e.g., Nix et al. really let their parameters be determined essentially so as to fit the spectra near ^{208}Pb and a few other doubly-closed shell regions. The different predictions as to the size of the $Z = 114$ and $N = 184$ gaps may be compared in fig. 21 and fig. 22. To the right in these figures you see the spectra predicted from Hartree–Fock calculation by Vautherin et al. [26] and by Köhler [27]. By far the greatest uncertainty in SHE predictions lies in all probability in this extrapolation of the shell-model potential parameters to new and distant mass regions.

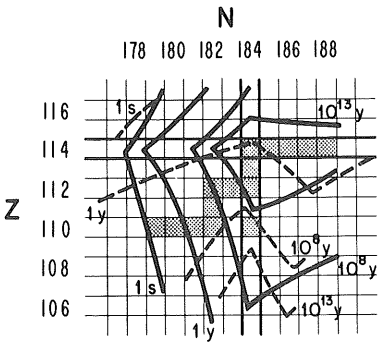

Fig. 20. Nuclear half-lives for the SHE island in terms of spontaneous fission (solid lines), alpha decay (dashed lines). Beta stable elements are denoted by cross-shaded squares.

The very long half-lives obtained by Pauli, Strutinsky et al., though modified by the inclusion of the alpha decay mode, is hardly congruent with the great scarcity of super-heavy elements found in nature. If any at all, there may be just two SHE nuclei found, both of them detected in the nuclear emulsion tracks and emanating from cosmic rays. Pauli et al. anticipate the nasty question of why so little is around of these elements by suggesting the name Old Gorm to the $Z = 114$ element, referring to an old Danish king resting in his grave inactive but always present. Pauli may even have had the mythical Holger Danske in mind, who from under the vaults of Helsinor's castle abides the day when the old Viking king is to make Denmark great again. The problem is then, Should there not be more radioactive fringe elements (if there are such long-lived elements at the center of the island) in the more intermediate range of half-lives, and furthermore readily detectable?

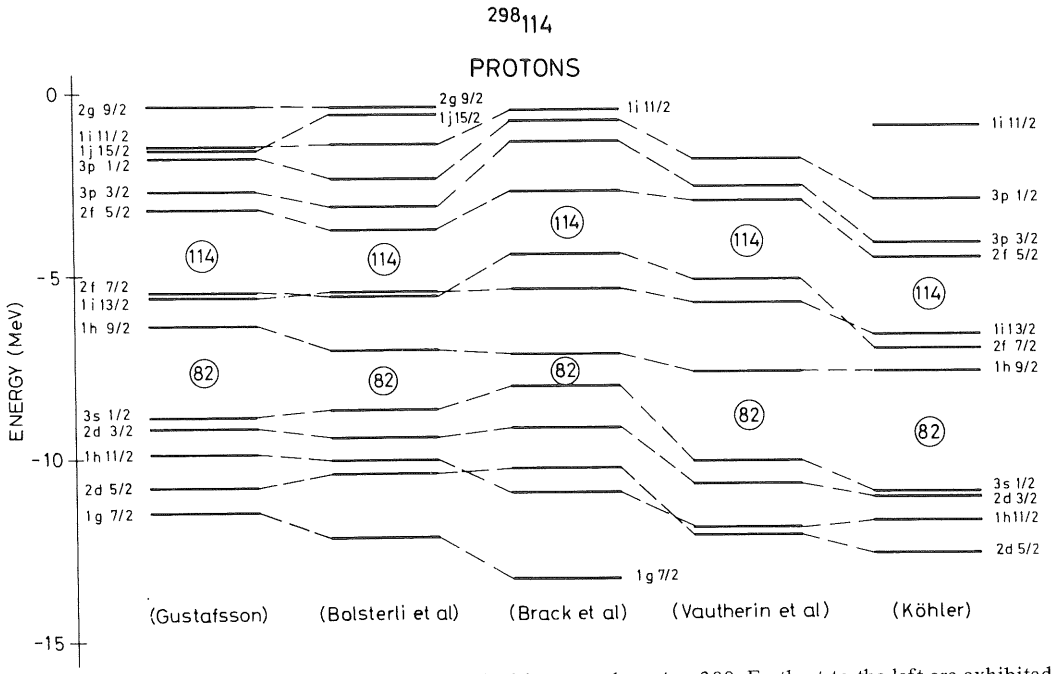

Fig. 21. Single-proton orbitals for spherical shapes for nuclei with mass values $A \approx 300$. Farthest to the left are exhibited levels of the present modified-oscillator model, next the predicted schemes of Bolsterli et al. and Damgaard et al. based on Woods–Saxon type potentials. To the right the level schemes obtained in calculations based on two-body interactions are shown. Note that the $Z = 114$ gap largely reflects the predicted spin–orbit splitting between the f 7/2 and f 5/2 orbitals.

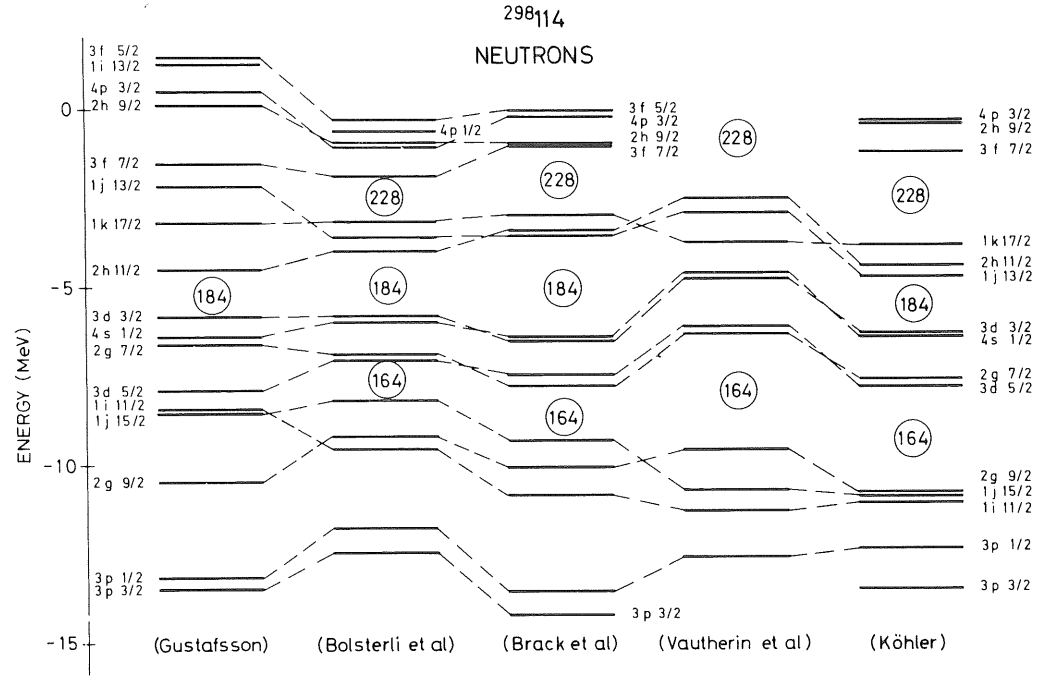

Fig. 22. Same as fig. 21 but valid for neutron levels. Note that the calculations by Vautherin et al. do not predict any gap connected with $N = 184$.

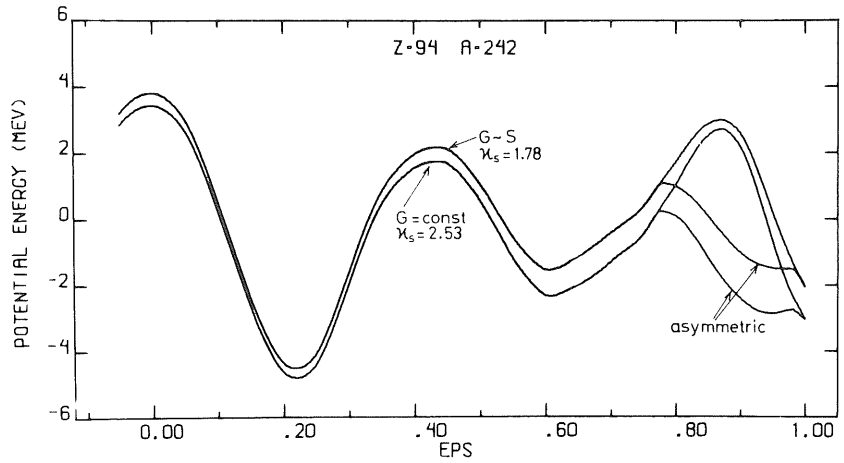

Fig. 23. The projected fission barrier of ^{242}Pu as a function of the elongation parameter ϵ (ϵ_4, ϵ_3, ϵ_5). Both the waist-line and asymmetry coordinates are thus included when the energy for each ϵ is minimized with respect to the other coordinates. The barrier is calculated under two alternative assumptions (1) G being proportional to the surface area and κ_s equal to 1.78, (2) G assumed constant and κ_s equal to 2.53.

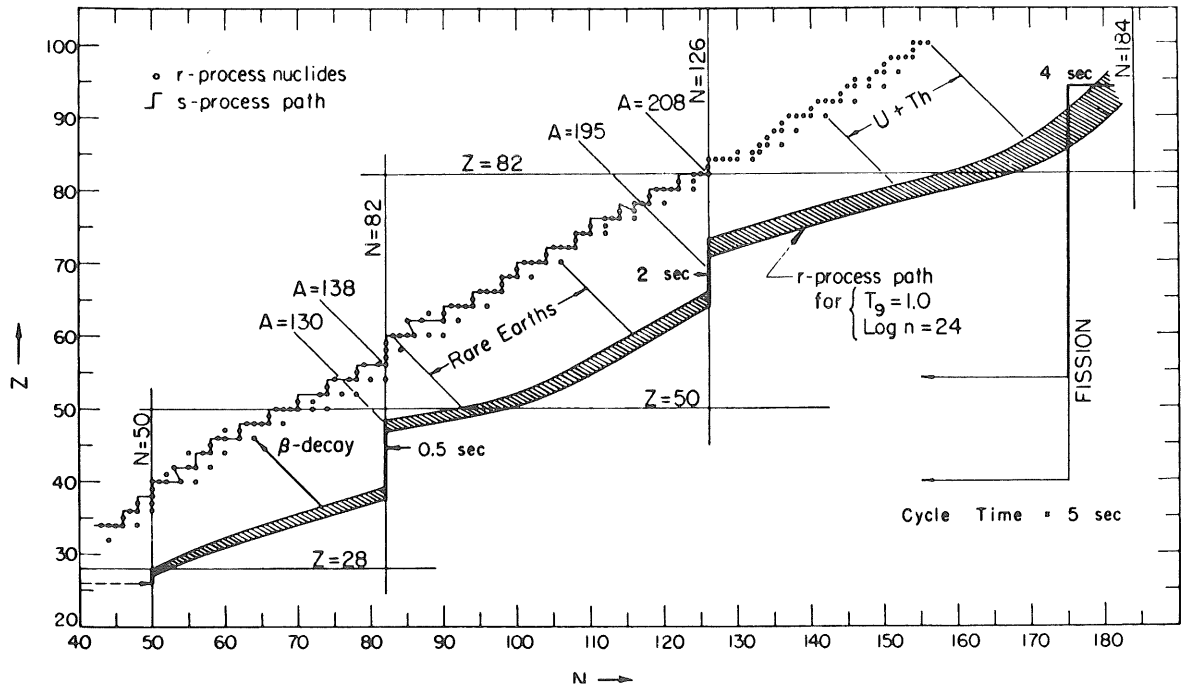

Fig. 24. Element synthesis in stars according to the r- and s-process respectively, according to earlier calculations by Seeger [29]. Fission here terminates before $N = 184$ is reached.

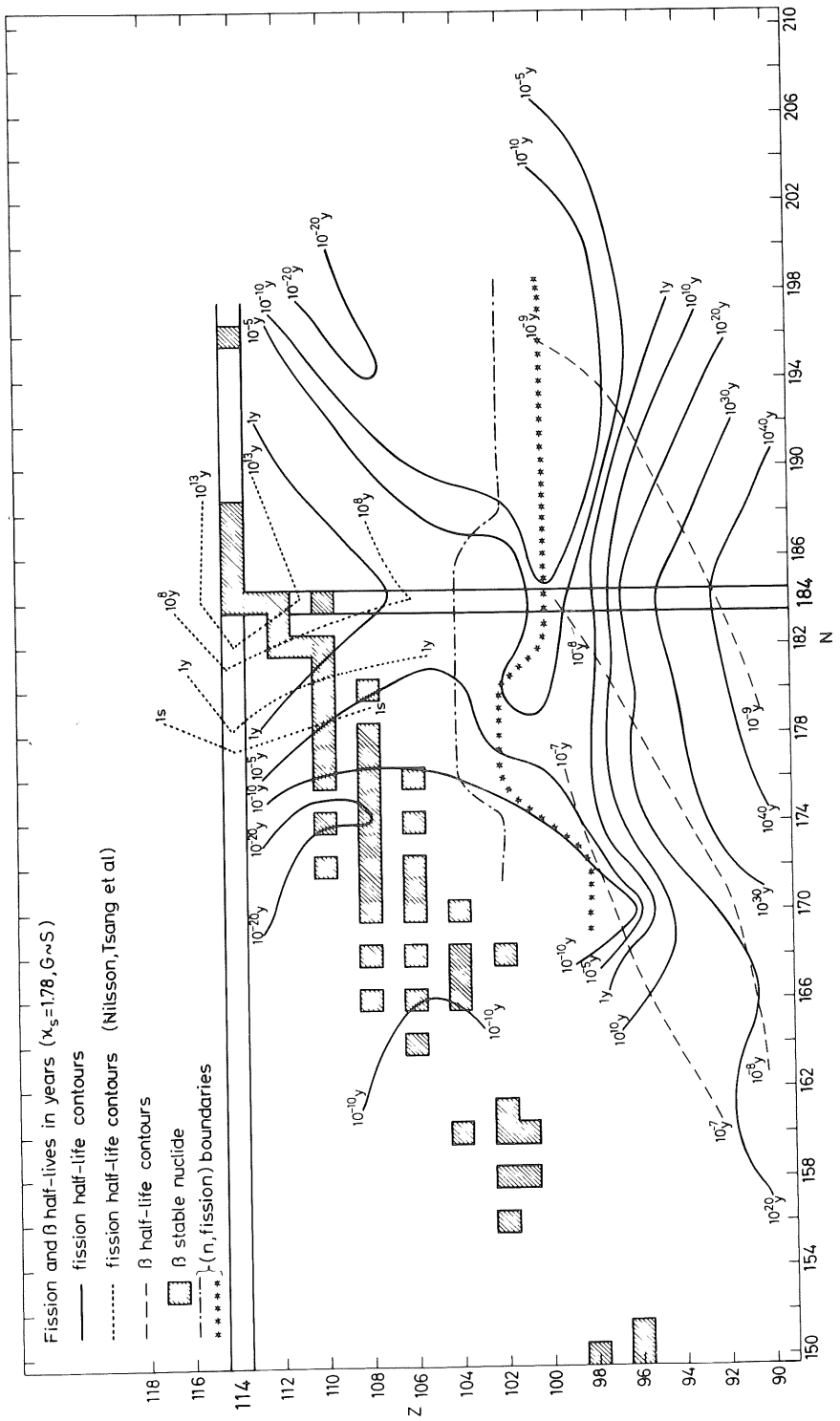

Fig. 25. Theoretical half-lives of elements calculated by R. Boleu [30] on the basis of the present model along r-process path with respect to spontaneous fission (solid lines), beta-decay (dashed lines). Beta-stable elements in regions calculated are given by shaded squares. Limiting lines for dominance of neutron-induced fission over gamma decay according to two variants described in the text are marked by dot–dashed and cross–hatched lines. Note that the path to the SHE island appears impassible. The corresponding calculations are based on the assumptions G being proportional to the surface area and $\kappa_s = 1.78$.

Actually ^{244}Pu with a half-life of 80 million years (or nearly the same as that predicted for ^{294}110 by Tsang and myself and our co-workers) was recently detected by chemical means from terrestrial ores by the Los Alamos nuclear chemists. I believe, in case the truth is closer to the predictions by Pauli, Strutinsky et al. than to our predictions, that you have to say that the r-process of element synthesis, which is considered responsible for the terrestrial quantities for ^{244}Pu, ^{238}U, etc., probably fails to make any SHE's. To look a little into that problem we have been studying fission barriers for very neutron rich actinide elements, over a range of N values extending from about 160 up and beyond 190. The predictions turn out to be very sensitive to the knowledge of the liquid-drop parameters and in particular to the value of the surface-symmetry term.

In the Myers–Swiatecki version of the liquid-drop model the parameters are fitted not just to reproduce masses but also to give reasonable fission barriers. In particular the indeterminateness of the surface symmetry term may be taken as a measure of the arbitrariness in this fitting procedure.

The surface symmetry coefficient κ_s is chosen by Myers–Swiatecki [28] as 1.78 or to equal the volume symmetry coefficient. Seeger [29] instead determines the surface symmetry term independently, fitting masses only and not barriers, and ends up with a surface symmetry coefficient that in the MS formulation would correspond to $\kappa_s = 2.53$. We have now as an alternative (and also as a measure of our ignorance) also used the larger surface symmetry coefficient as a variant of the calculations. This must obviously result in a lowering of the actinide barriers as the surface energy is weakened. To still retain on the average the observed actinide barriers we have replaced the assumption of G proportional to the surface area with the assumption of G = constant, which latter assumption may better reproduce the more recent interpretation of data as to the level density above the highest of the fission barrier peaks. As seen in fig. 23 as in figs. 19 approximately the same barriers are obtained for the actinides with the two alternative parameter sets.

The picture is dramatically changed, however, as we now proceed to discuss the nuclei as calculated by Boleu [30] from our group. The reduction due to the change in κ_s is thus considerable even when the compensatory change in the assumption about the pairing matrix element is introduced at the same time. The corresponding estimated fission half-lives are given in a critical region of the r-process path in figs. 25 and 26. In fig. 25 the following decay processes have been included, spontaneous and induced fission, alpha- and beta-decay. Of these processes alpha half-lives are too long to affect the region of r-process nuclei and are neglected in the figure. Spontaneous fission half-lives are indicated by solid lines. The $10^{-10}y$ isochrone appears to terminate the r-process path at $Z \approx 100$, $N \approx 190$ from which point the subsequent beta-decay process (with half-lives marked by dashed lines) fails to reach the super-heavy island. Any progress along the thin bridge of half-lives in excess of $10^{-5}y$ appears blocked by a line referring to induced fission. Along this line induced fission half-lives equal the half-lives of gamma-decay back to the ground state following neutron capture. (Two alternative lines, denoting "optimist" and "pessimist" estimates are indicated, both effectively blocking the passage.) Similar S.F. half-life estimates for the alternative κ_s assumption are exhibited in fig. 26 resulting in even shorter half-lives.

The asymmetry effect is not included in these estimates. From the available cases it appears that the reduction due to asymmetry can be expected to give rise to a reduction factor between 10^2 and 10^5. The inclusion of this effect would thus make the r-process path terminate for even smaller A-values.

It must be emphasised, that the conclusions obtained are indeed very sensitive to the estimate of the shell correction function connected with $N = 184$. The latter gap comes out smaller on the basis of the modified oscillator model than in terms of other single-particle potentials employed.

The r-process path recently suggested by Schramm and Fowler [31], is shown in fig. 27. However, the Schramm and Fowler path is based on fission and alpha half-life estimations in terms of semi-empirical half-life formulas. The shell correction term entering the fissility value x is partially based on empirical information available in the actinide region while for the extrapolation to the super-heavy region the results of our 1968 calculations [19] have been utilized. Our recent calculations here referred to cast considerable doubt on the procedure followed by Fowler et al., parametrizing the fission process in terms of a semi-

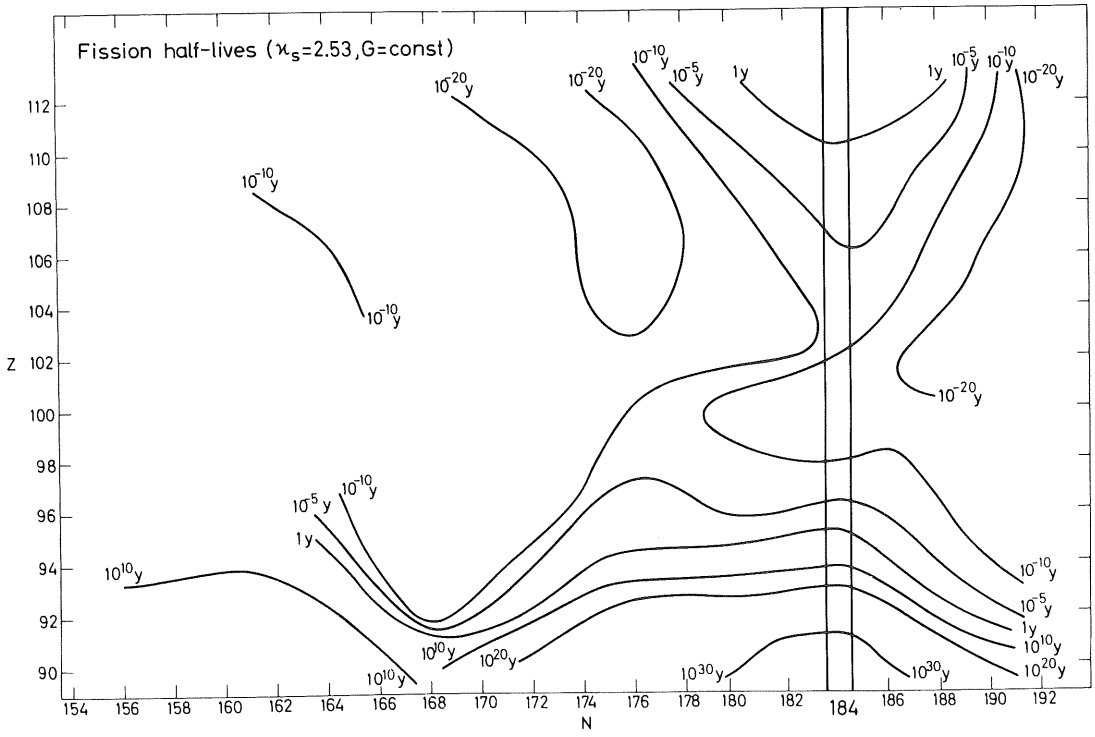

Fig. 26. Fission half-lives calculated for the alternative assumption G = const. and κ_S = 2.53. Note the generally shorter half-lives relative to those of fig. 25.

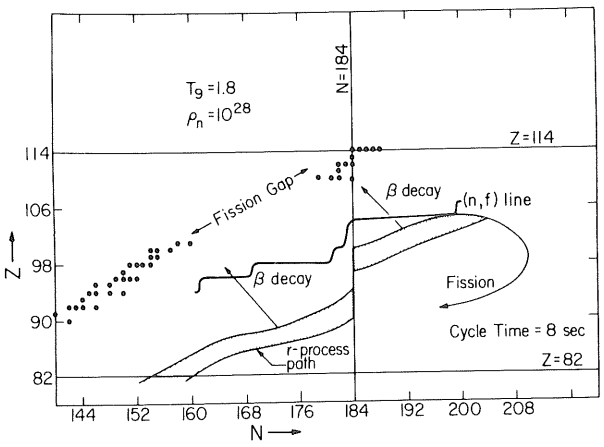

Fig. 27. Path or r-process according to recent calculations by Schramm and Fowler [31]. Note that contrary to the results of the theoretical calculations of figs. 25 and 26 the r-process proceeds from N = 184 and $Z \approx 98$ toward $N \approx 200$ and $Z \approx 106$, from which passage the SHE island could be populated.

empirical fissility value. Such an effective fissility value to us appears hardly sufficient to reproduce the complex features of a two- or three-peak barrier.

Acknowledgements

I am indebted to my co-workers S.E. Larsson, R. Bengtsson, I. Åberg and R. Boleu for helping me collect the most recent information on the subject and supplying me with their unpublished results.

References

[1] J. Rainwater, Phys. Rev. 79 (1950) 432.
[2] P. Brix and H. Kopfermann, Z. Physik 126 (1949) 344.
[3] A. Bohr, Kgl. Danske Videnskab. Selskab Mat. Fys. Medd. 26 (1952) no. 14.
[4] G.N. Flerov and S.M. Polikanov, Compt. Rend. Congres Intern. de physique nucléaire, Paris, 1964 (CNRS, Paris, 1964) Vol. 1, p. 407.

[5] V.M. Strutinsky, Yad. Fiz. 3 (1966) 614; (Soviet J. Nucl. Phys. 3 (1966) 449).
[6] J.R. Nix, Ann. Rev. Nucl. Sci. 22 (1972) to be published; M. Bolsterli, E.O. Fiset, J.R. Nix and J.L. Norton, Phys. Rev. C5 (1972) 1050.
[7] M. Brack, J. Damgaard, H.C. Pauli, A. Stenholm-Jensen, V.M. Strutinsky and C.Y. Wong, Rev. Mod. Phys. 44 (1972) 320.
[8] V.V. Pashkevich, Nucl. Phys. A169 (1971) 275.
[9] B.L. Andersen, F. Dickman and K. Dietrich, Nucl. Phys. A159 (1970) 337.
[10] B. Slavov, J.E. Galonska and A. Faessler, Phys. Letters 37B (1971) 483.
[11] P. Holzer, U. Mosel and W. Greiner, Nucl. Phys. A138 (1969) 241.
[12] T. Johansson, Nucl. Phys. A183 (1972) 33.
[13] S.E. Larsson, I. Ragnarsson and S.G. Nilsson, Phys. Letters 38B (1972) 269.
[14] U. Götz, H.C. Pauli and K. Alder, Nucl. Phys. A175 (1971) 481; Phys. Letters 39B (1972) 436.
[15] V.V. Pashkevich, Nucl. Phys. A133 (1969) 400.
[16] A. Bohr and B.R. Mottelson, Nuclear structure, Vol. 2 W.A. Benjamin, New York, to be published).
[17] L.G. Moretto, Phys. Letters 38B (1972) 393.
[18] C.F. Tsang, Lawrence Radiation Laboratory Report, UCRL-18899 (1969).
[19] S.G. Nilsson, C.F. Tsang, A. Sobiscewski, Z. Szymanski, S. Wycech, G. Gustafson, I.L. Lamm, P. Möller and B. Nilsson, Nucl. Phys. A131 (1969) 1.
[20] P. Möller and S.G. Nilsson, Phys. Letters 31B (1970) 283.
[21] C.F. Tsang and J.B. Wilhelmy, Nucl. Phys. A184 (1972) 417.
[22] G. Gustafson, P. Möller and S. G. Nilsson, Phys. Letters 34B (1971) 349.
[23] S. Björnholm and J.E. Lynn, Rev. Mod. Phys., to be published.
[24] P. Möller, Nucl. Phys., to be published.
[25] H.C. Pauli and T. Ledergerber, Nucl. Phys. A175 (1971) 545.
[26] D. Vautherin, M. Véneroni and D.M. Brink, Orsay preprint FPNO/TH 193 (1970).
[27] H.S. Köhler, Nucl. Phys. A170 (1971) 88.
[28] W.D. Myers and W.J. Swiatecki, Arkiv Fysik 36 (1967) 343.
[29] P.A. Seeger, Proc. 3rd Intern. Conf. on Atomic Masses, Winnipeg, 1967 (Univ. Manitoba Press, Winnipeg, 1967) p. 85.
[30] R. Boleu, S.G. Nilsson, R. Sheline and K. Takahashi, Phys. Letters B40 (1972) 517.
[31] D.N. Schram and W.A. Fowler, Nature 231 (1971) 103.